GA–A25615

A GYROTRON-POWERED PELLET ACCELERATOR FOR ITER

by
F.W. PERKINS and P.B. PARKS

SEPTEMBER 2006

GENERAL ATOMICS

DISCLAIMER

GA–A25615

A GYROTRON-POWERED PELLET ACCELERATOR FOR ITER

by
F.W. PERKINS and P.B. PARKS

This is a preprint of a paper to be presented at the 21st IAEA Fusion Energy Conference, October 16-21, 2006, in Chengdu, China, and to be published in the *Proceedings.*

GENERAL ATOMICS PROJECT 40010
SEPTEMBER 2006

GENERAL ATOMICS

Gyrotron-Powered Pellet Accelerator for ITER: Improvements and Experiments

F.W. Perkins 1) and P.B. Parks 1)

1) General Atomics, San Diego, California, USA

e-mail contact of main author: perkins@fusion.gat.com

Abstract. Assessments of design modifications of the gyrotron-powered pellet accelerator show that issues raised by the initial design can be eliminated by appropriate design changes. These include: (1) Use of an annular guide tube which separates the mm-wave waveguide function from the pellet guide-tube function will eliminate low density gas breakdown from the mm-wave guide. (2) A calculation concludes that the mm-wave electric fields, while strong, are nonetheless well-below breakdown because of the high density of solid hydrogen. (3) The ITER thermal-engineering design should make provisions for mounting the annular guide-tube on the thermal shield which will passively cool the guide tubes. Microwave heating of the thermal shield will be less than 1% of the total heat load. (4) A mobile tamper, transparent to mm-waves, can eliminate the need for moving parts in the tokamak interior. Tamper recoil energy and momentum will be used to operate the loading of pellet cartridges but only well outside the tokamak chamber. Several experiments to test these ideas are outlined. With a minimum of engineering redesign, speed of ITER pellets could increase by an order of magnitude. An improved ablation model finds this increases the ablation penetration length by a factor-of-six.

1. Introduction

As tokamak plasma parameters approach those of ITER, the need for independent control of core plasma density and thermonuclear reaction rates becomes evident. Most contemporary tokamaks regulate density by pumping or by gas puffing. Ionization then occurs in a thin layer at the plasma surface leading in turn to a strong correlation between core density and that of the scrape-off-layer (SOL) which must accommodate the heat flux emanating from the core. In the plasma core, density sources can act to control the shape of the density profile and consequently the thermonuclear energy production.

For ITER, the injection of high-speed DT-ice pellets is the key technique proposed for refueling and active control of core density [1]. Upon entering the core plasma, high speed pellets become ionized by an ablation process wherein the ionization rate is affected by a self-shielding cloud of evaporated neutral particles [2,3]. It is evident that the greater the pellet speed, the greater the distance it will go before ablation turns it into a neutral gas cloud and then into a plasma. One can define an ablation penetration distance which must increase as pellet speed increases. Arguments that the ablation length increases slowly with increasing pellet velocity ($\propto V^{1/3}$) are based on a linear temperature profile. More realistic profiles with a pedestal electron temperature approach the V scaling of a flat temperature profile.

Conventional pellet accelerators are large devices and not suitable for operations in the interior regions of even an ITER-class facility. Consequently DT-ice pellets in contemporary experiments are accelerated remotely and propagate to the their launch point in guide tubes which have one or more 90° bends. Experiments at Oak Ridge National Laboratory (ORNL) [4,5] find that DT-ice pellets in bends of $R = 1$ m curvature, fracture when velocities V exceed 200 m/s. This result is in accord with the physics picture of centrifugal force stresses exceeding the yield stress

$$\rho V^2 (h/R) > \sigma \quad . \tag{1}$$

Here, ρ denotes the mass density of DT-ice, $\rho \approx 250$ kg/m^3, $\sigma \approx 0.2$ MPa, pellet size h = 0.01 m, R is the curvature radius $R \approx 1.0$ m. Images show that, the larger the velocity, the smaller fractured pellets bits become – in accord with (1). Overall the ORNL experiments demonstrate that pellets can propagate intact in curved guide tubes, but their velocity will be limited by Eq. (1). Fragmentation does not affect the mobile tamper system (described below) because of the much higher yield stress $\sigma \sim 10^5$ MPa of tamper material.

Fueling a tokamak by injection of DT ice pellets is generally regarded as a two-step process. The first step and the subject of this contribution is the ionization of the neutral pellet material into a cold dense plasma, but one in which the flux-surface-averaged pressure remains constant. The key issue is: How far into the plasma can the pellet penetrate before it becomes completely ionized? This length is called the ablation penetration length and is dependent on the pellet speed and size as well as background plasma density and temperature. From an operational point-of-view, the ablation rate determines the initial conditions for the subsequent MHD flows [6,7] which, in turn, govern whether the ablated plasma will show strong toroidal effects or will be constrained to pedestal region.

This analysis of ablation penetration combines a database of ionization rates [8], etc. with model temperature profiles and pellet velocity v. For these calculations, we have assumed an electron temperature with a pedestal value T_p and a central value T_o

$$T_e = T_p\left(1-\frac{x}{a}\right)+\left(\frac{x}{a}\right)T_o \quad , \tag{2}$$

where x denotes length inward from the High-Field-Side (HFS) separatrix. Since the ablation rate is a strong function of T_e [Eq. (3)], it is important to assess the role of the pedestal temperature. For the H-mode plasmas anticipated in ITER, ablation is a weak function of electron density n_e which can be taken to be constant $n_{14} \approx 1$.

The starting point is the pellet ablation rate formula developed by Parks [2] for an assumed spherical pellet

$$r_p^{2/3}\frac{d}{dt}r_p = -\frac{8.2\cdot 10^{15}\ \ n_e^{1/3}T_e^{11/6}}{4\pi n_c(2^{1/3})\left[\ell n\left(\frac{2T_e}{I^*}\right)\right]^{2/3}} \quad , \tag{3}$$

here r_p denotes the radius of the pellet material that remains un-ionized. The physics of pellet ablation is contained in Eq. (3) which expresses ablation physics in terms penetration lengths. Formula (3) is in eV-cm units. When converted to $n_{14} = n_e/10^{14}$, keV units and using $n_c = 3.2\cdot 10^{22}$ cm^{-3} atomic for hydrogen isotopes and, $[ln(2T_e/I^*)]^{2/3} = 3.4$, the scaling formula becomes

$$\frac{d}{dt}r_p^{5/3} = -58.0\ \ n_{14}^{1/3}T_p^{11/6}\left[(1-vt/a)+(vt/a)(T_o/T_p)\right]^{11/6} \quad . \tag{4}$$

A simple integral yields the result

$$r_p^{5/3} = r_{po}^{5/3} - 58.0\cdot n_{14}^{1/3}T_p^{11/6}\left(\frac{1}{v}\right)\frac{aT_p}{T_o-T_p}\left(\frac{6}{17}\right)\left[\left(1+\left(\frac{x}{a}\right)\frac{(T_o-T_p)}{T_p}\right)^{17/6}-1\right] \quad , \tag{5}$$

where $x = vt$ is the penetration distance, V denotes the pellet velocity, and r_{po} is the radius of the pellet as it enters the plasma. The penetration distance is defined as the point where $r_p = 0$. Equation (5) can be solved directly for x in terms of $a^* = a\, T_p/(T_o - T_p) \approx a/4$.

$$\frac{x}{a^*} = \left[1 + \frac{17}{6}\left(\frac{r_{po}^{5/3} v}{T_p^{11/6} 58\ (n_{14})^{1/3} a^*}\right)\right]^{6/17} - 1 \quad , \tag{6}$$

The initial radius r_{po} of the sphere is given by the requirement that the pellet mass be a fixed fraction $\eta \approx 0.1$ of the plasma mass

$$\frac{4\pi}{3} r_{po}^3 = 4\pi^2 \eta\ Ra^2 \frac{n_{14}}{n_c} \quad , \tag{7}$$

where an elongation $\kappa = 2$ has been assumed. It is evident that there are two ranges governing the penetration as a function of pellet velocity – the linear low-velocity range and the high-velocity $v^{6/17}$ range, which has been found in previous studies. To separate these two velocity ranges, we introduce a characteristic velocity v^* such that Eq. (5) simplifies to

$$\frac{x}{a^*} = \left[1 + \frac{v}{v^*}\right]^{6/17} - 1 \quad , \qquad v^* = \frac{(1.1 \cdot 10^5\,\text{cm/s})\ T_{p,\text{keV}}^{11/6}\ a}{\eta^{5/9} n_{14}^{2/9} \left(Ra^2\right)^{5/9}} \quad . \tag{8}$$

As an example of applications, Table 1 gives the penetration length for high-speed and low-speed ITER scenarios as well as an example for DIII-D. The pellet speed of 300 m/s is the limit above which centrifugal force fragments the pellet propagating in curved guide tube.

The plasma deposited by the ablation process as summarized in Table 1 constitutes the initial conditions for the hydromagnetic flows [6,7] that strongly differentiate between HFS and LFS launch. No adjustable constants have been introduced by this analysis; only a single overall rate determined in Eq. (3) has been used. All temperatures, densities, etc. appear quite reasonable, engendering confidence in the scaling properties.

Table 1. Penetration Examples

Parameter/Tokamak	ITER Low-Speed	ITER High-Speed	DIII-D	DIII-D (Nondimensionally ITER Low-Speed)
$T_{ped,\,keV}$	3.0	3.0	1.0	1.0
Minor radius (cm)	200	200	67	67
Pellet mass fraction	0.1	0.1	0.1	0.1
R/a	3	3	3	3
V* (m/s)	450	450	130	130
Pellet speed	300	3000	300	87
Normalized penetration	0.2	1.3	0.52	0.2
x/a* penetration (cm)	10	65	8.3	3.3

Consider the ITER case. At the nominal design point, penetration lengths for ITER reported in Table 1 are sensitive to pedestal temperature and pellet velocity. They amount to a significant benefit for pellet velocities of 3000 m/s or higher. The nominal value of v = 300 m/s planned for the ITER design has a quite short penetration length – 10 cm – close to the projected H-mode pedestal width. It could well complicate establishment of an H-mode edge. But with high-speed, inside-launch the penetration length is 65 cm. This improvement with high-speed, inside-launch is a result of ITER lying between the $v^{1/3}$ and v scaling regimes. An opportunity exists to reliably improve ITER fueling.

It would be elucidating to construct in DIII-D a discharge nondimensionally (from an ablation perspective) identical to the low-speed ITER discharge. The key nondimensional parameter is v/v^* and Table 1 shows a pellet speed v = 87 m/s for the DIII-D discharge makes v/v^* identical in the DIII-D and Low-Speed ITER discharges. The common ablation penetration length is 0.05 *(minor radius).

Once the pellet has become ionized and deposited as a spike of plasma, its subsequent evolution is governed by hydromagnetic flows. Observations show and theory supports strong toroidal effects [6,7]. Plasma deposited on the low field side generated outward flows and an appreciable fraction ~30% of the pellet was swept out by the flows. On the other hand, toriodal effects on flows initiated by high field side deposition swept the plasma inward and are consistent with unity fueling efficiency [9]. For conventional pellet accelerators, high field side launch requires guide tubes with 90° bends and can not benefit from pellet velocities exceeding those of Eq. (1). For low field side launch, guide-tube bends are not required and appreciably higher velocities can be used. But, the fuelling inefficiently remains and is unacceptable for a reactor.

It would appear that a key choice must be made, high field side deposition with constrained velocity but excellent fueling efficiencies versus low field side deposition with high pellet velocity but poor fuelling efficiency.

This work describes a new pellet accelerator configuration that avoids such a choice by locating the accelerator itself on the high field side, while retaining the simplicity of LFS injectors. A general description can be found in Ref. [10]. The key observation is that ITER is so large that a pellet injector acceleration tube can be placed in the slot between blanket shield modules. The shear size of ITER coupled with several new design features, including a layered pellet, have been combined into a pellet gun-accelerator that can be located on the inside midplane and aimed directly outward. The power needed to drive the gun is generated remotely by a gyrotron and delivered by a mm-wave waveguide. The pellets still must be guided by tubes, which run adjacent to the mm-wave waveguide, but they are small, ≈0.02 m diameter, and can be constrained to low velocity so that fracture is not an issue.

The original design for gyrotron-powered plasma guns has been published [10]. This is reviewed in Sec. 2. Section 3 addresses critiques of the original design in the key areas of breakdown and automatic operation and outlines the design revisions they motivated. Section 4 sets forth an experimental plan to check elements and validate scaling predictions. A fully integrated test could be carried out on DIII-D. Section 5 concludes that, with minimal engineering complications, ITER could implement a high-pellet-velocity fueling capability without fracture while retaining the favorable flows of high-field-side fueling. The anticipated velocities exceed present capabilities by an order of magnitude.

2. The Gyrotron-Powered Pellet Accelerator

The goal for the Gyrotron-Powered Pellet Accelerator (GPPA) is to develop a gun-configuration accelerated pellet source that can be used for tokamak refueling. Figure 1 illustrates the path that adjacent waveguide/guide-tubes take, starting from their source, continuing along the ITER thermal shield, and finally making a 90° bend with curvature radius $R = 0.25$ m to align with the outward major radius direction. Equation (1) will be fulfilled for pellets provided their velocity V remains V < 100 m/s. The guide tube is annular, the inner tube guiding the pellets.

The outer annular channel guides the gyrotron power to the interaction region which is fixed in space. Both the waveguide termination region and the tamper contain reflecting mm-wave optics. For the proper tamper position, the mm-wave power is directed into the pusher region where it heats the tamper gas – in direct analogy to gun powder ignition

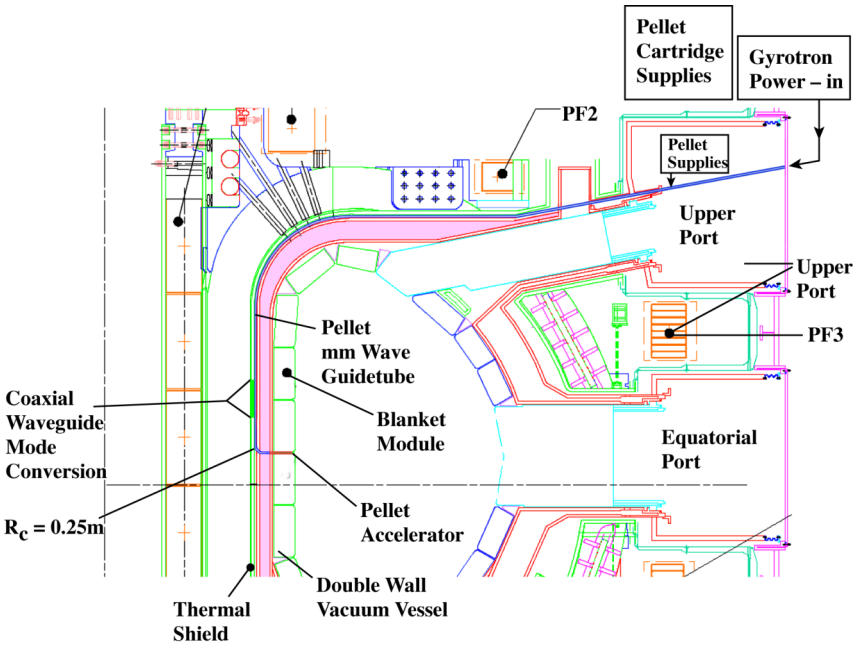

FIG. 1. Layout of pellet injection system. Pellet cartridges are introduced through the upper port and propagate along the thermal shield.

The pellets used are not simple blobs of DT. In fact, the pellets are sophisticated carefully layered material with much in common with rifle cartridges. Figure 2 illustrates an annular guide-tube configuration consisting of two cylindrical shells. The inner shell contains a mobile tamper which can translate freely along the tube axis. Its position will be monitored by laser diagnostic sightlines. The tamper fits snugly in the inner tube and is composed of very high resistivity dielectric material so that it is transparent to millimeter waves. The outside portion of the annular guide tube is the mm-wave waveguide which is fixed in the laboratory frame.

The heating of the pusher gas is controlled by its conductivity and would be small if the pusher gas were simply D_2. To achieve more-or-less uniform heating of the pusher region, a suspension of fine beryllium or graphite spherical dust is added to the pusher gas. These particles are sufficiently large so the skin depth is small and surface currents flow to exclude the mm-wave magnetic field from the dust-particle core. The resistive dissipation of these currents heats the D_2. This technique enables one to control the conductivity of the D_2 gas and leads to more-or-less uniform heating in the pusher region.

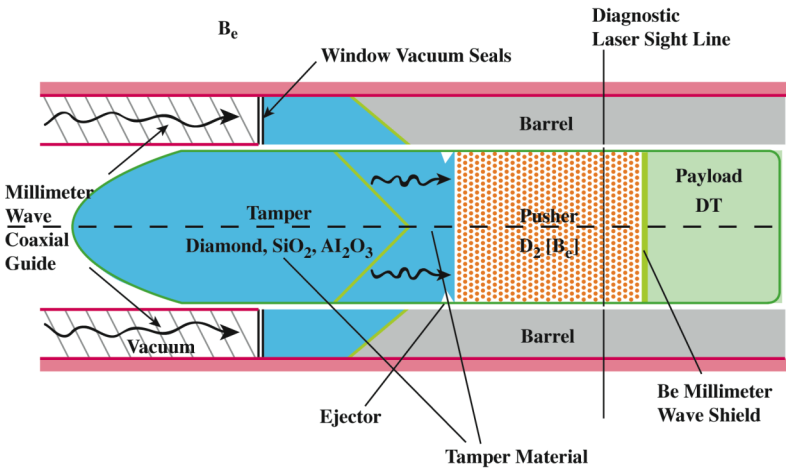

FIG. 2. Structure of the pellet cartridge. The movable tamper-pusher-payload assembly fits snuggly, yet slides freely, along the barrel of the tube.

For gyrotron sources of ~1 MW, heating occurs slowly compared to sound travel times and plasmas expand as the entropy/mass increases by the gyrotron heating. The pressure of the hot D_2 gas accelerates the payload which is shielded from mm-wave power by a beryllium film. An accurate summary of the results gives [10]

$$V = 1.0\,(PL/M_p)^{1/3} \quad , \tag{9}$$

in SI units. Here, P is the gyrotron power, L the accelerator length, V the pellet velocity, and M_p the pellet mass.

Pusher gas pressure also drives the tamper backward with equal but opposite momentum along the guide-tube where it can be captured and its energy and momentum used to eject the spent cartridge and load in a fresh one. The parameters are close to those in machine gun technology. http://science.howstuffworks.com/machine-gun.htm.

An innovative element of this system is the propagation of the energy through the tamper and its absorption by micron-sized dust particles which we are free to choose. This permits one to use a gun design (rather than a less efficient rocket principle).

3. Design Improvements

Dual use of a single guide tube for both pellets and for mm-wave power was a key feature of the original design [10]. The tube both guided pellets to their launch points on the HFS and propagated gyrotron power into the pusher chamber raising its pressure. But since the tamper is mobile, the vacuum seal between the pusher chamber and the guide tube would not be perfect, permitting high-pressure pusher-gas leakage into the waveguide. Low-pressure breakdown would ensue. To avoid breakdown, an annular guide tube is proposed wherein the outer wave guide section guides the mm-wave power and, as depicted by Fig. 2, is isolated from the inner annular section by a hard mm-wave window. The inner annular tube section serves as a pellet guided tube and guides the mobile tamper assembly.

A simple breakdown criterion using a uniform plasma model has been devised. The very high angular frequency (~10^{12} s^{-1}) makes conventional breakdown theory inappropriate. Let us first summarize the magnitude of electric fields and fluid variables required for circular waveguide of diameter d = 0.005 m to transmit a power of 1 MW at 170 GHz – the technology being developed for ITER. The corresponding power density $4.0\cdot10^{10}$ watts/m^2 = E^2/η_o gives an electric field of 4 MV/m. Also of interest are the quiver velocity for electrons $v = eE/m\omega = 7.0\cdot10^5$ m/s, the corresponding kinetic energy $u_o = (eE)^2/(2m\omega^2) = 1.4$ eV, and quiver displacement $x_o = (eE)/(m\omega^2) = 5.0\cdot10^{-7}$m. Representative pressure in the pusher gas chamber rises to ~100 MPa.

The very high angular frequency $\omega \approx 10^{12}$ rad/s has an important consequence: Electrons cannot gain sufficient energy in a wave half-period to affect ionization rates. Breakdown will not occur as a result of energy gain of a single electron but as a thermal instability in which the electron temperature rises by an energy diffusion process.

Electron-neutral collisions are the dominant collision process and we assume its value is given by [11]

$$\nu_n = n_n \sigma \left(\frac{T_e}{m}\right)^{1/2} \qquad \sigma = 5.0\cdot10^{-19}\ \mathrm{m}^2 \quad , \tag{10}$$

For nominal discharge parameters $n_n = 3.2 \cdot 10^{28}$ m^{-3}, $\sigma = 5.0 \cdot 10^{-19}$ m^{-3}, $T_e = 1000$ K, and $\nu_n = 1.7 \cdot 10^{17}$ s^{-1} >> ω. This justifies a dc, uniform plasma model to examine thermal stability. The resistive heating by the wave electric field is $jE = (n_e e^2 E^2)(m\nu_n)^{-1}$ while the inelastic cooling rate is $n_e \nu_n (2\, m/M)\, (T_e - T_n)$. The mass ratio enters because the collisions of light electrons with heavy molecules are almost elastic. Equating the heating and cooling rates gives

$$jE = \left(\frac{n_e e^2 E^2}{m\ \nu_n} \right) = n_e \nu_n \left(\frac{2m}{M} \right) (T_e - T_n) \quad . \tag{11}$$

Straightforward algebra leads to the stability criterion

$$\left(\frac{eE}{p} \right) < \sigma \left(\frac{2m}{M} \right)^{1/2} \qquad p = n_n T_e \quad . \tag{12}$$

For the parameters of our experiment, $E = 24$ MV/m, a factor of 2 above the estimated value from power flux. It is interesting that this simple model gives the E/p scaling of breakdown observations.

The heated pusher gas also accelerates the tamper to equal but opposite momentum. It will move backward along the inner annular region and be recovered. Tamper energy and momentum can be used to eject spent cartridges and load fresh ones. There is much in common with machine gun technology (http://science.howstuffworks.com/machine-gun.htm).

The adjacent guide tubes should be attached to the vacuum vessel thermal shield which will passively cool them. The thermal load of the heat shield 190 kW [12], while the time-average mm wave power is only several hundred watts. We conclude that extra heat loads from pellet injectors are negligible.

4. Integrated Test on DIII-D

An integrated test of the ITER fueling system could be carried out on DIII-D with all dimensions scaled a factor-of –3 smaller. Thus, the accelerating tube will be 0.15 m long in outward major radius and be fed by an annular guide tube with a 0.10 m curvature bend. This adds up to a required 0.25 m separation between the separatrix and wall, which will be obtained by moving the major radius outward. Figure 3 shows a representative equilibrium with the required 25 cm separation between the separatrix and vessel walls. Table 2 shows the specifics of these parameters. It does have an aspect ratio closer to that of ITER than DIII-D. A limiter will protect the accelerating tube in this region. The pellets will have a diameter of 0.03 m. A gyrotron with frequency $\nu \approx 300$ GHz and a millisecond pulse duration will be needed, but only at lower power $P \approx 100$ kW and low duty cycle.

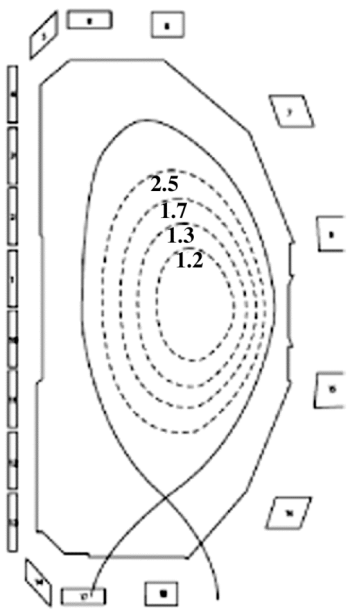

FIG. 3. Representative DIII-D equilibrium with 20 cm available on inboard midplane for gyrotron powered pellet injector.

Table 2. Scaling of Pellet Injection from ITER to DIII-D

Parameter	ITER	DIII-D	Comments
R, a	6.0, 2.0 (m)	2.0, 0.67 (m)	Factor-of-3; linear in length
Blanket/shield, accelerating tube length	0.45 (m)	0.15 (m)	Linear in length
Atomic density	$n_e = 1.0 \times 10^{20}$ m^{-3}	$n_e = n_{20} \times 10^{20}$ m^{-3}	Representative density for DIII-D
Pellet diameter d (mm)	9.0	3.0	Matches pellet atomic inventory
Pellet fraction η atomic inventory	0.3	0.3	η = constant is a scaling principle
Accelerator length (m)	0.45	0.15	Simulates ITER blanket/shield
Accelerator tube diameter d (mm)	9.0	3.0	Matched to pellet size
Pellet mass $M_p = \rho d^3 \eta(\pi/4)$ $\eta = 200$ kg/m-3	2×10^{-4} η kg	3×10^{-6} η kg	Pellet is constant fraction of discharge mass
Required power $P = M_p V^3/L$	(0.9 MW) V km/s^3	(20 kW) V km/s^3	Estimated from scaling relation; large ITER pellets ablate slowly
Desired output velocity V	2-5 km/s	2-5 km/s	Supports factor-of-5 increase in ablation length
Gyrotron frequency ν is twice the waveguide cutoff frequency	$\nu = 76$ GHz	$\nu = 302$ GHz	Smaller size means increased frequency; note power is small for DIII-D; ~300 GHz under development
Scaling of required power density	9.0×10^9 V km/s^3 W/m^2	3.0×10^9 V km/s^3 W/m^2	Power density almost independent of size
Pellet repetition rate	0.1 s^{-1}	30 s	Pellet rate needed to maintain density

5. Conclusions

Ablation, toroidicity, and pellet speed all affect fueling of ITER and form the basis of control by pellet injection. This report finds that the redesigned gyrotron-powered pellet injector should not be subject to either low-density or high-density breakdown and yields pellet speeds of 3 km/s – an order of magnitude above present plans and sufficient to alter the MHD flows. The impact on ITER engineering would be minimal, but the adjacent annular guide tubes should be provided from the outset.

References

[1] MILORA, S., *et al.,* Nucl. Fusion **35** (1995) 657.
[2] PARKS, P.B., and ROSENBLUTH, M N., Phys. Plasmas **5 (1998)** 1380.
[3] BAYLOR, L.R., *et al.,* Phys. Plasmas **12 (2005)** 056103.
[4] COMBS, S.K., *et al.,* Fusion Technology **34** (1998) 419.
[5] COMBS, S.K., *et al.,* Fusion Engineering and Design **58-59** (2001) 343.
[6] PARKS, P.B., and BAYLOR, L.R., Phys. Rev. Lett. **94** (2005) 125002.
[7] LANG, P.T., *et al.,* Nucl. Fusion **40** (2000) 245.
[8] BAYLOR, L.R., *et al.,* Nucl. Fusion **37 (1997)** 445.
[9] LANG, P.T., *et al.,* Nucl. Fusion **42** (2002) 388.
[10] PARKS, P.B., and PERKINS, F.W., Nucl. Fusion **46** (2006) 770; US Patent Application filed October 21, 2005.
[11] NRL Plasma Formulary (1994) p. 39.
[12] IAEA, ITER Technical Basis, Chapter 2.8 (2002) p. 11.